© 2016. Published by The Company of Biologists Ltd | Development (2016) 143, 2965-2972 doi:10.1242/dev.139485

RESEARCH REPORT

Tmem2 regulates cell-matrix interactions that are essential for muscle fiber attachment

Lucile Ryckebüsch, Lydia Hernandez, Carole Wang, Jenny Phan and Deborah Yelon*

ABSTRACT

Skeletal muscle morphogenesis depends upon interactions between developing muscle fibers and the extracellular matrix (ECM) that anchors fibers to the myotendinous junction (MTJ). The pathways that organize the ECM and regulate its engagement by cell-matrix adhesion complexes (CMACs) are therefore essential for muscle integrity. Here, we demonstrate the impact of *transmembrane protein 2* (*tmem2*) on cell-matrix interactions during muscle morphogenesis in zebrafish. Maternal-zygotic *tmem2* mutants (*MZtmem2*) exhibit muscle fiber detachment, in association with impaired laminin organization and ineffective fibronectin degradation at the MTJ. Similarly, disorganized laminin and fibronectin surround *MZtmem2* cardiomyocytes, which could account for their hindered movement during cardiac morphogenesis. In addition to ECM defects, *MZtmem2* mutants display hypoglycosylation of α-dystroglycan within the CMAC, which could contribute to the observed fiber detachment. Expression of the Tmem2 ectodomain can rescue aspects of the *MZtmem2* phenotype, consistent with a possible extracellular function of Tmem2. Together, our results suggest that Tmem2 regulates cell-matrix interactions by affecting both ECM organization and CMAC activity. These findings evoke possible connections between the functions of Tmem2 and the etiologies of congenital muscular dystrophies, particularly dystroglycanopathies.

KEY WORDS: Zebrafish, Muscle morphogenesis, Extracellular matrix, Cardiac fusion

INTRODUCTION

In vertebrates, most skeletal muscles derive from precursors found within the somites, repetitive segments of paraxial mesoderm that flank the embryonic notochord (Bryson-Richardson and Currie, 2008; Buckingham and Vincent, 2009). As muscle precursors mature, they elongate to form fibers that span each segment and attach to the somite boundaries (Goody et al., 2015). Attachments are created through direct interactions of muscle fibers with the extracellular matrix (ECM), and sites of attachment develop into the myotendinous junction (MTJ), which transmits muscular forces to the skeletal system (Charvet et al., 2012). Thus, cell-matrix connections facilitate the morphology, integrity and function of developing muscles. In contrast, failure to maintain fiber attachments can lead to the progressive tissue degeneration that underlies muscular dystrophy. Although numerous causative mutations have been associated with congenital muscular dystrophies (Bertini et al., 2011; Kirschner, 2013), our understanding of the molecular mechanisms that regulate muscle fiber attachment remains incomplete.

Several protein complexes are known to play primary roles in connecting muscle cells to the MTJ (Charvet et al., 2012; Goody et al., 2015; Thorsteinsdóttir et al., 2011). Within the ECM, deposition of both fibrillar fibronectin and polymerized laminin is crucial for successful anchoring of muscle fibers. These ECM molecules are engaged by a variety of transmembrane receptors at fiber termini, including integrin heterodimers and the dystrophin-associated glycoprotein complex (DGC). In collaboration with cytoplasmic proteins such as focal adhesion kinase (FAK) and paxillin, these receptors form cell-matrix adhesion complexes (CMACs) that link the extracellular environment to the cytoskeleton and thereby facilitate both force transmission and signaling. Whereas the importance of ECM and CMAC components is well documented, it is less clear how deposition of the ECM is controlled or how CMAC assembly is regulated in order to insure appropriate cell-matrix interactions.

The use of the zebrafish as a model organism provides valuable opportunities for interrogating the functions of genes involved in muscle fiber attachment (Berger and Currie, 2012; Gibbs et al., 2013). Here, we show that the zebrafish gene *transmembrane protein 2* (*tmem2*) plays an important and previously unappreciated role in regulating cell-matrix interactions at the MTJ. Tmem2 is a type II transmembrane protein with a small cytoplasmic domain, a single-pass transmembrane domain and a large ectodomain (Smith et al., 2011; Totong et al., 2011). Prior studies have demonstrated that *tmem2* regulates the regional restriction of the cardiac atrioventricular canal (Smith et al., 2011; Totong et al., 2011). In addition, embryos lacking both maternal and zygotic supplies of *tmem2* (*MZtmem2*) exhibit earlier defects in multiple tissues, including aberrantly shaped somites (Totong et al., 2011). Through analysis of the somite defects in *MZtmem2* mutants, we find that loss of *tmem2* function leads to muscle fiber detachment. Our results indicate that *tmem2* is required for appropriate ECM deposition during skeletal muscle morphogenesis, as well as for deposition of the ECM that surrounds cardiomyocytes during heart tube formation. In addition, *tmem2* promotes the glycosylation of α-dystroglycan within the DGC at the MTJ. Thus, our studies suggest that Tmem2 impacts cell-matrix interactions by influencing both the organization of the ECM and the post-translational modification of the CMAC.

RESULTS AND DISCUSSION

Loss of *tmem2* function leads to muscle fiber detachment

Our previous studies indicated that zebrafish embryos lacking both maternal and zygotic supplies of *tmem2* (*MZtmem2*) exhibit abnormal somite morphology, whereas embryos lacking only maternal supplies of *tmem2* (*Mtmem2*) are indistinguishable from wild-type (Fig. 1A,D) (Totong et al., 2011). Notably, instead of the

Division of Biological Sciences, University of California, San Diego, La Jolla, CA 92093, USA.

*Author for correspondence (dyelon@ucsd.edu)

L.R., 0000-0001-7927-2006; L.H., 0000-0001-5883-9325; C.W., 0000-0003-4717-3024; J.P., 0000-0002-1894-2560; D.Y., 0000-0003-3523-4053

Received 8 May 2016; Accepted 11 July 2016

Development (2016) 143, 2965-2972 doi:10.1242/dev.139485

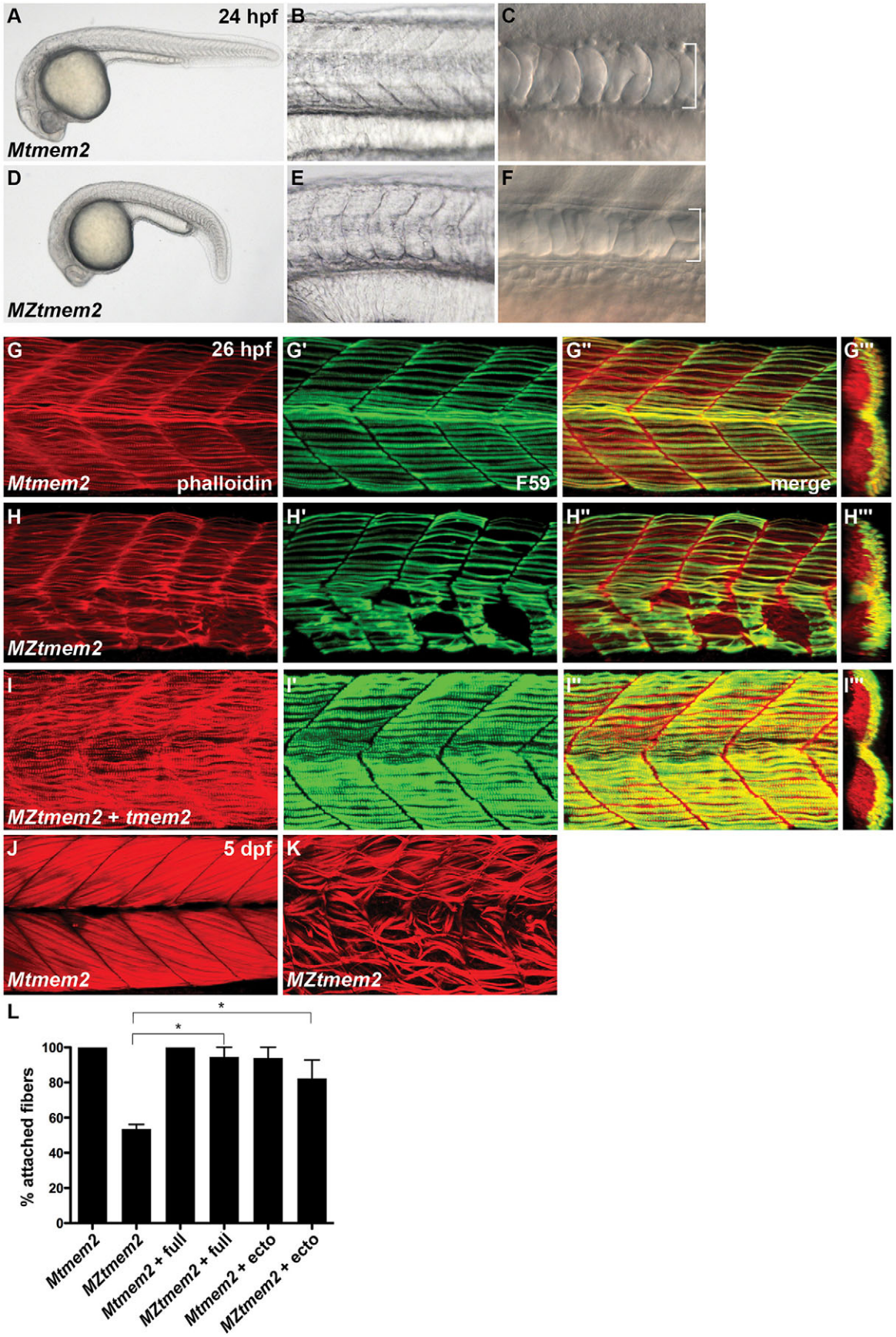

Fig. 1. See next page for legend.

Development (2016) 143, 2965-2972 doi:10.1242/dev.139485

Fig. 1. Disrupted muscle fiber attachment in *MZtmem2* mutants. (A-F) Lateral views display somite and notochord morphology at 24 hours post-fertilization (hpf). *Mtmem2* (A-C) control siblings are indistinguishable from wild-type. *MZtmem2* mutants (D-F) exhibit a normal number of somites (32 somites in A,D) but have U-shaped (E) rather than chevron-shaped (B) somites and a slightly narrow notochord (bracket, F). (G-K) Immunofluorescence reveals muscle fiber organization, using Phalloidin (red) to recognize both fast and slow fibers and F59 (green) to recognize slow fibers; lateral views with dorsal up (except for transverse views in G‴-I‴) at 26 hpf (G-I) or 5 days post-fertilization (dpf) (J,K). *MZtmem2* mutants display muscle fiber detachment (H-H″), whereas *Mtmem2* siblings exhibit normal fiber attachment (G-G″). Attachment can be rescued in *MZtmem2* mutants by injection of wild-type *tmem2* mRNA (I-I″; *n*=6/7). The severity of detachment in *MZtmem2* mutants increases over time (K), indicating the importance of *tmem2* for the maintenance of muscle fiber attachment. (L) Bar graph compares average prevalence of fiber attachment in somites at 48 hpf; error bars indicate s.e.m. $F59^+$ fibers were counted within 11 somites of multiple embryos [*Mtmem2*, *n*=6; *MZtmem2*, *n*=4; *Mtmem2* expressing full-length *tmem2* ('+full'), *n*=6; *MZtmem2*+full, *n*=8; *Mtmem2* expressing *tmem2* ectodomain ('+ecto'), *n*=2; *MZtmem2*+ecto, *n*=5]. Introduction of either full-length Tmem2 or the Tmem2 ectodomain into *MZtmem2* mutants caused improvement in fiber attachment. Asterisks indicate significant differences from *MZtmem2* (Student's *t*-test; $P<0.001$ for full, $P<0.05$ for ecto). See also Table S1.

chevron-shaped somites seen in *Mtmem2* embryos, *MZtmem2* mutants display U-shaped somites (Fig. 1B,E). Formation of chevron-shaped somites requires Hedgehog signaling from the notochord (Barresi et al., 2000; Blagden et al., 1997); however, the morphology, integrity and differentiation of the *MZtmem2* notochord appear relatively normal (Fig. 1C,F; Fig. S1B,D). Moreover, the *MZtmem2* somite shape does not seem to result from defective Hedgehog signaling, since *ptc1* expression appears to be intact in *MZtmem2* mutants (Fig. S1A,C).

We investigated whether defects in muscle fiber morphogenesis could underlie the aberrant somite shape in *MZtmem2* mutants. *MZtmem2* embryos exhibit a normal number of somites (Fig. 1A,D) and have no apparent defects in initial somite boundary formation (Fig. S2A,B). However, muscle fiber attachment defects are prevalent in *MZtmem2* mutants (Fig. 1G,H). Both fast and slow fibers show detachment from the MTJ (Fig. 1H; Fig. S3); in addition, some muscle fibers aberrantly cross the MTJ (Fig. 1H). Fiber detachment becomes more widespread as development proceeds (Fig. 1J,K; Fig. S4A,B), indicating failure to properly maintain attachments. Consistent with this, although zygotic *tmem2* (*Ztmem2*) mutants exhibit normal somite morphology at early stages, defects in somite shape and muscle fiber integrity emerge in some *Ztmem2* mutants over time (Fig. S4C-G), presumably as maternal supplies of *tmem2* are depleted. Together, these results provide the first demonstration that *tmem2* plays an important role in preserving muscle fiber attachment to the MTJ.

Tmem2 regulates organization of basement membrane components

Establishment and maintenance of muscle fiber attachment at the MTJ require successful interactions with the ECM molecules that compose the basement membrane (Goody et al., 2015; Snow and Henry, 2009). Moreover, the *MZtmem2* phenotype shares some characteristics with the phenotypes of laminin-deficient and fibronectin-deficient embryos, including the presence of fibers that cross the MTJ (Snow et al., 2008a,b), prompting us to investigate the ECM in *MZtmem2* mutants. Instead of the normally concentrated deposition of laminin at the MTJ in *Mtmem2* embryos (Fig. 2A,C), we observed diminished and poorly organized laminin in *MZtmem2* mutants (Fig. 2B,D), particularly in locations where fibers were detached (Fig. 2D). In contrast, fibronectin deposition appears relatively robust, albeit somewhat disorganized, in *MZtmem2* mutants (Fig. S2A-F; Fig. 2E,F). During the usual progression of muscle morphogenesis (Snow and Henry, 2009; Jenkins et al., 2016), fibronectin levels degrade at the MTJ over time (Fig. 2E,G), in conjunction with accumulation of laminin (Fig. 2A,C). However, in *MZtmem2* mutants, fiber attachment defects are accompanied by aberrantly increased fibronectin localization (Fig. 2F,H). This may represent a secondary consequence of laminin deficiency, since organized laminin has been shown to play an indirect role in facilitating fibronectin degradation at the MTJ (Jenkins et al., 2016); alternatively, increased fibronectin could be a secondary response to muscle fiber detachment, akin to the increased fibronectin fibrillogenesis seen in association with some myopathies (Hori et al., 2011; Rampoldi et al., 1986; Zacharias et al., 2011).

The deficient and disorganized ECM at the *MZtmem2* MTJ made us wonder whether ECM defects could account for other aspects of the *MZtmem2* mutant phenotype. *MZtmem2* mutants exhibit cardia bifida, reflecting an early failure of cardiac morphogenesis (Totong et al., 2011). In wild-type embryos, bilateral populations of cardiomyocytes move toward the midline, where they meet and merge to assemble the heart tube through a process called cardiac fusion. *MZtmem2* mutants fail to execute cardiac fusion and instead display two separated groups of cardiomyocytes in bilateral positions (Fig. 3F,G) (Totong et al., 2011). The composition of the basement membrane has a potent influence on cardiac fusion: either diminished or excessive ECM deposition can inhibit cardiomyocyte movement (Arrington and Yost, 2009; Garavito-Aguilar et al., 2010; Trinh and Stainier, 2004). Interestingly, the ECM adjacent to the *MZtmem2* myocardium exhibits irregular and disorganized deposition of both laminin and fibronectin (Fig. 3A-E), which could account for the failure of cardiac fusion in *MZtmem2* mutants. Thus, our data suggest that Tmem2 regulates both cardiac and skeletal muscle morphogenesis via modulation of the ECM.

The Tmem2 ectodomain can perform some aspects of Tmem2 function

Since the biochemical function of Tmem2 is currently unknown, it remains unclear whether this protein could exert its influence on the basement membrane through direct interaction with ECM components. To evaluate whether the Tmem2 ectodomain is sufficient to execute its functions, we replaced the transmembrane and cytoplasmic domains of Tmem2 with a signal peptide and tested whether this modified version of Tmem2 can rescue the *MZtmem2* mutant phenotype. Injection of wild-type *tmem2* mRNA into *MZtmem2* mutants can rescue both muscle fiber attachment (Fig. 1I,L; Table S1) and cardiac fusion (Fig. 3F-K; Table S2). Similarly, we found that the Tmem2 ectodomain can also ameliorate both of these features of the *MZtmem2* phenotype, although less efficiently than full-length Tmem2 (Fig. 1L; Tables S1 and S2). Therefore, the Tmem2 ectodomain can mediate at least some of the molecular functions of Tmem2, consistent with a model in which Tmem2 functions within the extracellular environment.

Tmem2 influences glycosylation of α-dystroglycan

Our results suggest that the muscle fiber detachments in *MZtmem2* mutants could be a direct consequence of faulty ECM organization. Since fiber attachment also relies upon effective CMAC assembly (Goody et al., 2010, 2015; Jackson and Ingham, 2013), we investigated whether the MTJ defects in *MZtmem2* mutants are restricted to the basement membrane or are also reflected in the

Development (2016) 143, 2965-2972 doi:10.1242/dev.139485

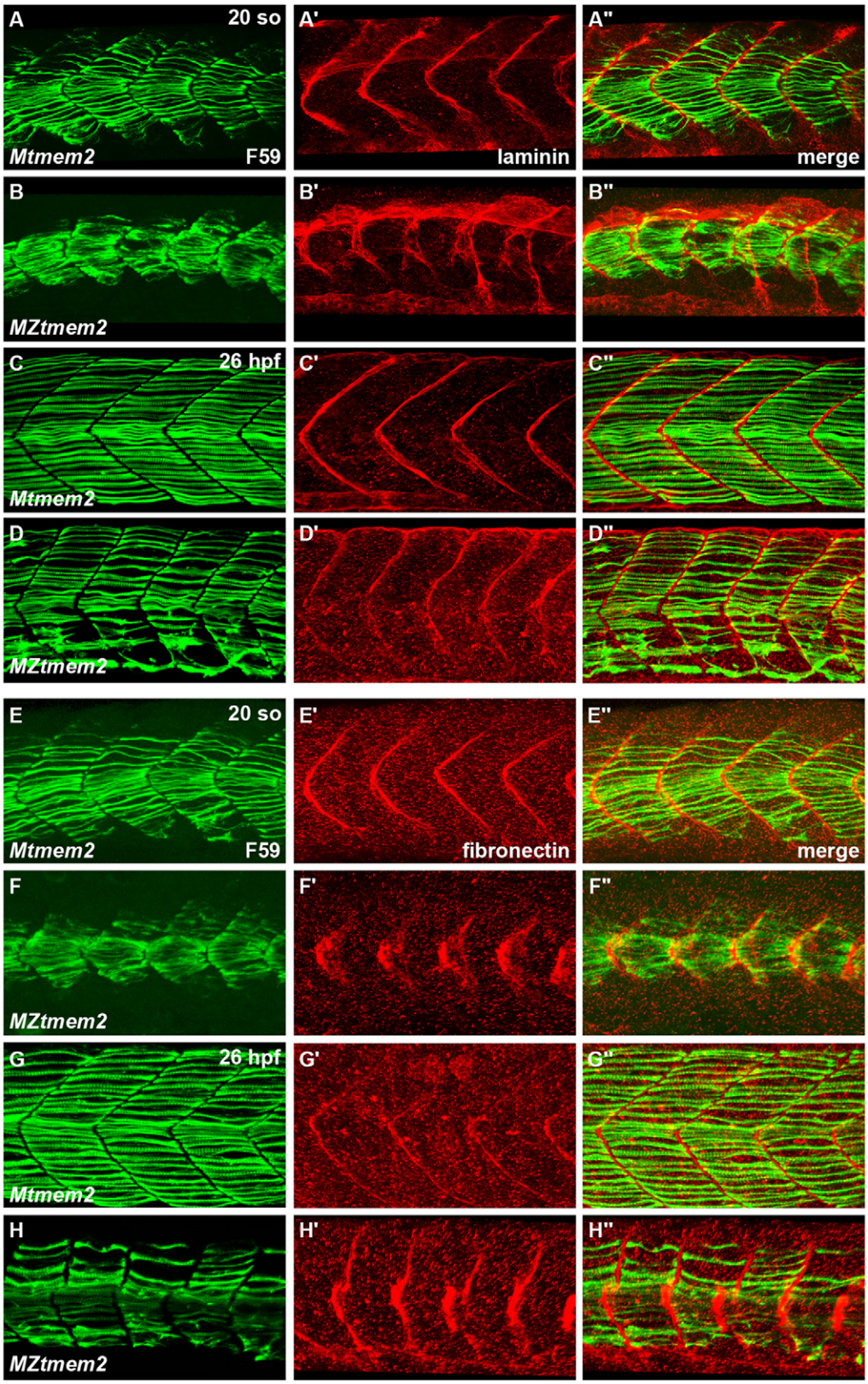

Fig. 2. Aberrant ECM organization at the MTJ in *MZtmem2* mutants. (A-H) Immunofluorescence indicates localization of laminin (red, A′-D′) and fibronectin (red, E′-H′) relative to slow muscle fibers, labeled with F59 (green, A-H); lateral views, dorsal up, at 20 somite stage (so) (A,B,E,F) and 26 hpf (C,D,G,H). (A-D) Laminin is present at the *MZtmem2* MTJ by 20 so (B), although it appears disorganized compared with localization in *Mtmem2* siblings (A). By 26 hpf, laminin deposition appears diminished at the *MZtmem2* MTJ (D). (E-H) Fibronectin fibrillogenesis is evident at the *MZtmem2* MTJ at 20 so (F), albeit in an aberrant pattern that echoes the morphology of the *MZtmem2* somites. By 26 hpf, when much of the fibronectin has been degraded at the *Mtmem2* MTJ (G), fibronectin levels appear increased in *MZtmem2* mutants (H), particularly where fibers are detached. However, nearly all of this fibronectin degrades in *MZtmem2* mutants by 40 hpf (data not shown).

localization of CMAC components. Examination of three components of the DGC – the scaffolding protein paxillin, a phosphorylated form of focal adhesion kinase (pFAK), and the core complex component β-dystroglycan (βDG) – demonstrated that each was localized to the MTJ in *MZtmem2* mutants (Fig. 4A-F). However, the distribution of each component was affected: paxillin was not properly concentrated (Fig. 4A,B), pFAK levels appeared to be reduced (Fig. 4C,D) and some gaps in βDG localization were observed (Fig. 4E,F). These aberrations could reflect ineffective CMAC assembly as a result of poor ECM engagement, or they

Development (2016) 143, 2965-2972 doi:10.1242/dev.139485

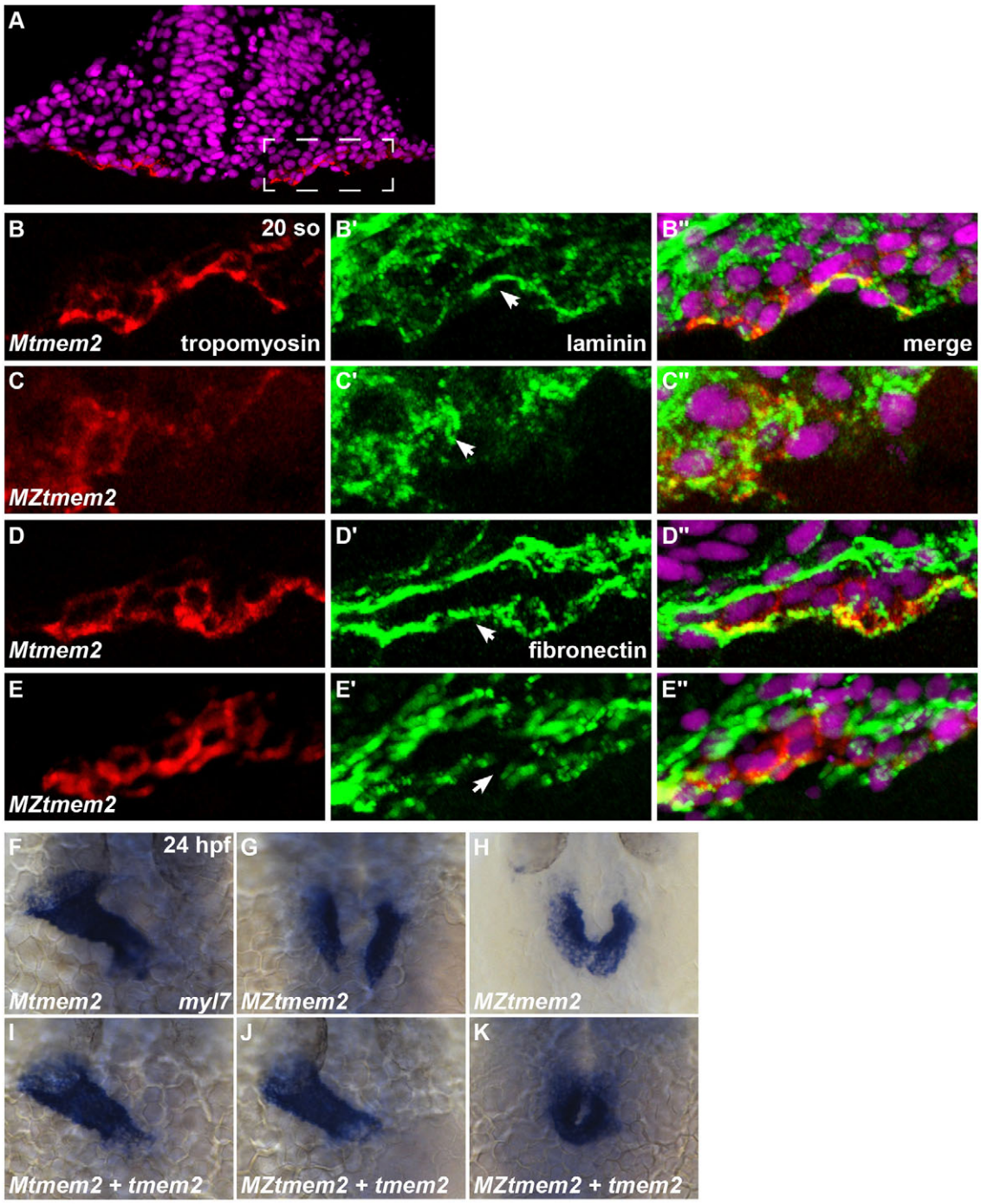

Fig. 3. ECM disorganization accompanies cardia bifida in *MZtmem2* mutants. (A-E) Immunofluorescence illustrates laminin (green; B′,C′) and fibronectin (green, D′,E′) localization near the myocardium (marked by tropomyosin in red); transverse sections, dorsal up, at 20 so, with DAPI (magenta). Dashed rectangle in A indicates the right cardiac primordium, closer views of which are shown in B-E. (B) During cardiac fusion, laminin deposition is normally evident on the basal side of the myocardium (arrowhead, B′) (Arrington and Yost, 2009). (C) In *MZtmem2* mutants, laminin organization appears severely compromised (arrowhead, C′) and a discrete basal layer does not form. (D,E) Fibronectin fibrils normally underlie the myocardium during cardiac fusion (arrowhead, D′) (Trinh and Stainier, 2004), but fibronectin deposition appears irregular and disorganized in *MZtmem2* mutants (arrowhead, E′). (F-K) Expression of *myl7* at 24 hpf in *Mtmem2* (F,I) and *MZtmem2* (G,H,J,K) siblings; dorsal views, rostral up. By 24 hpf, the heart tube assembles normally in *Mtmem2* siblings (F), but *MZtmem2* mutants typically exhibit cardia bifida (G). Occasionally, *MZtmem2* mutants display partial cardiac fusion (H, Table S2). Injection of *tmem2* mRNA rescues cardiac fusion (K) in *MZtmem2* mutants and can even restore heart tube formation (J, Table S2), but does not affect heart formation in *Mtmem2* siblings (I, Table S2).

could represent CMAC displacements that are secondary to fiber detachment (Bassett et al., 2003; Jacoby et al., 2009). Together, these observations suggest that recruitment of CMAC components to the MTJ does not require Tmem2, but that Tmem2 influences CMAC organization and integrity.

Our analysis of dystroglycan localization at the *MZtmem2* MTJ also revealed a significant defect in the glycosylation of α-dystroglycan (αDG) (Fig. 4E,F). Dystroglycan is post-translationally cleaved into two subunits, αDG and βDG (Moore and Winder, 2012). αDG functions as a laminin receptor and its

Development (2016) 143, 2965-2972 doi:10.1242/dev.139485

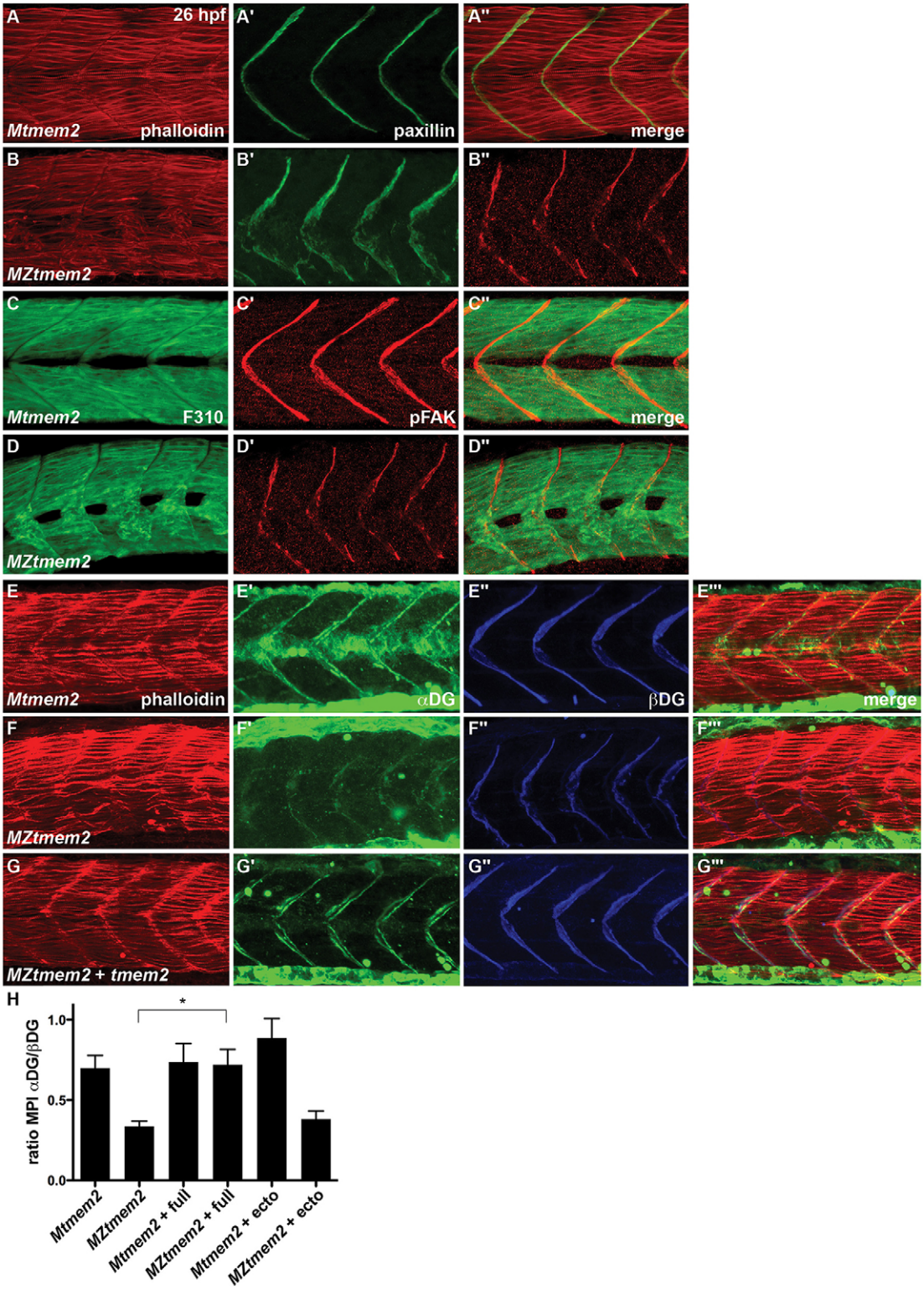

Fig. 4. Abnormal distribution and glycosylation of CMAC components in *MZtmem2* mutants. (A-G) Immunofluorescence shows localization of paxillin (green; A,B), pFAK (pY^{397}) (red; C,D), βDG (blue; E-G), and glycosylated αDG (green; E-G) relative to muscle fibers, marked with Phalloidin (red; A,B,E-G) or the antibody F310 (green; C,D); lateral views, dorsal up, at 26 hpf. (A-D) Both paxillin (B′) and pFAK (D′) are recruited to the *MZtmem2* MTJ. However, compared with the concentrated and robust localization in *Mtmem2* siblings (A′,C′), paxillin appears disorganized (B′), and pFAK levels are diminished (D′). (E-G) The antibody IIH6, which recognizes a glycosylated epitope of αDG within its laminin-binding site (Ervasti and Campbell, 1993), detects αDG at the MTJ in *Mtmem2* siblings (E′), but detects only trace amounts of glycosylated αDG at the *MZtmem2* MTJ (F′, Table S3). In contrast, βDG is readily detectable at the *MZtmem2* MTJ (F″). αDG glycosylation can be rescued in *MZtmem2* mutants by injection of *tmem2* mRNA (G′, Table S3). (H) Bar graph compares immunostaining intensity for glycosylated αDG, relative to levels of βDG, at the MTJ at 26 hpf; error bars indicate s.e.m. For each condition, we measured the mean pixel intensity (MPI) of immunostaining at five different MTJs in each of three representative embryos; see also Fig. S5. Introduction of full-length Tmem2, but not the Tmem2 ectodomain, caused improvement in αDG glycosylation in *MZtmem2* mutants. Asterisk indicates significant difference from *MZtmem2* (Student's *t*-test; $P<0.005$).

Development (2016) 143, 2965-2972 doi:10.1242/dev.139485

affinity for laminin depends upon its proper glycosylation (Sciandra et al., 2013). Strikingly, the glycosylated form of αDG is barely detectable at the *MZtmem2* MTJ, even though βDG localization is robust (Fig. 4F,H, Fig. S5C, Table S3). The influence of Tmem2 on αDG glycosylation may require its transmembrane and/or cytoplasmic domains: whereas full-length Tmem2 can rescue glycosylation in *MZtmem2* mutants, the Tmem2 ectodomain cannot (Fig. 4G,H, Fig. S5C, Table S3). Thus, in addition to its effects on ECM organization, Tmem2 promotes αDG glycosylation and, presumably, DGC activity, and this function of Tmem2 may employ a mechanism that is distinct from its other roles.

Tmem2 promotes cell-matrix interactions by influencing ECM organization and DGC modification

Together, our data establish Tmem2 as a previously unappreciated player in the cell-matrix interactions that control muscle morphogenesis. Tmem2 influences two distinct elements that enforce muscle fiber attachment: ECM deposition and CMAC composition. Since reduced laminin deposition interferes with fiber attachment (Goody et al., 2010; Hall et al., 2007; Jacoby et al., 2009; Snow et al., 2008b), it is likely that the ECM disruption in *MZtmem2* mutants contributes to their muscle defects. The onset of fiber detachment in *MZtmem2* mutants corresponds to the timeframe when laminin enrichment normally begins at the somite boundary (Crawford et al., 2003). Furthermore, ECM disorganization could explain the cardia bifida in *MZtmem2* mutants (Arrington and Yost, 2009; Garavito-Aguilar et al., 2010; Trinh and Stainier, 2004). In addition, since DGC glycosylation promotes its engagement of the ECM (Sciandra et al., 2013), hypoglycosylation of αDG could also contribute to the fiber detachments in *MZtmem2* mutants, as seen in embryos with reduced glycosyltransferase activity (Kawahara et al., 2010; Lin et al., 2011).

Do the ECM and CMAC features of the *MZtmem2* phenotype represent two separate functions of Tmem2, or are these roles of Tmem2 inter-related? Although composition of the ECM is not likely to have a direct impact on αDG glycosylation, prior studies have found that laminin organization can be influenced by DGC glycosylation state (Kanagawa et al., 2005; Michele et al., 2002). Alternatively, Tmem2 could influence the ECM and DGC through two independent mechanisms. In this regard, it is intriguing that the Tmem2 ectodomain can fulfill some, but not all, aspects of Tmem2 function: although the ectodomain can improve fiber attachment in *MZtmem2* mutants, it seems less effective than full-length Tmem2 and it cannot rescue αDG glycosylation. Thus, our data suggest that Tmem2 can function in the extracellular environment, consistent with our prior finding that myocardial expression of *tmem2* can non-autonomously rescue *MZtmem2* endocardial phenotypes (Totong et al., 2011). At the same time, our results suggest that functions of Tmem2 at distinct subcellular locations are relevant to its influence on post-translational modification of αDG. We therefore favor a model in which independent activities of Tmem2, affecting ECM organization and αDG glycosylation, collaborate to enforce muscle fiber attachment.

The influence of Tmem2 on muscle fiber attachment suggests an interesting link to the etiology of muscular dystrophy. In particular, Tmem2 may be relevant to the set of congenital muscular dystrophies known as dystroglycanopathies, which feature aberrant glycosylation of αDG (Muntoni et al., 2008; Wells, 2013). Mutations in 18 genes have been shown to cause dystroglycanopathies and several of these genes encode characterized or putative glycosyltransferases (Bouchet-Séraphin et al., 2015; Godfrey et al., 2011). However, as many as half of the dystroglycanopathy patients examined do not present mutations in known genes, and the process of post-translational modification of the DGC is not fully understood. Future elucidation of the molecular mechanisms of Tmem2 function is likely to provide valuable perspective on its relationship to dystroglycanopathy, as well as further insight into how ECM organization and CMAC composition both contribute to the stability of cell-matrix interactions during muscle development.

MATERIALS AND METHODS

Zebrafish

To obtain *MZtmem2* mutant embryos, we used germline replacement to generate chimeric female fish with a *tmem2*^{sk38} mutant germline and we bred these females to male *tmem2* heterozygotes, as previously described (Totong et al., 2011). *MZtmem2* mutants were distinguished from their *Mtmem2* siblings by morphological criteria and PCR genotyping (Totong et al., 2011). All zebrafish work followed protocols approved by the University of California, San Diego Institutional Animal Care and Use Committee (IACUC).

Immunofluorescence

Whole-mount immunofluorescence was performed as previously described (Goody et al., 2012), using Rhodamine Phalloidin (Invitrogen, R415) and antibodies listed in Table S4. For cryosections, embryos were fixed overnight in 4% paraformaldehyde at 4°C, followed by cryoprotection, mounting, sectioning, staining, and treatment with SlowFade Gold with DAPI (Invitrogen), as described previously (Garavito-Aguilar et al., 2010).

In situ hybridization

In situ hybridization for *ptc1* (ZDB-GENE-980526-196), *ehh* (ZDB-GENE-980526-135) and *myl7* (ZDB-GENE-991019-3) was performed as previously described (Yelon et al., 1999).

Injection

Embryos were injected at the one-cell stage with 200 pg mRNA encoding either full-length Tmem2 (Totong et al., 2011) or a modified version of the Tmem2 ectodomain. In this fusion protein, we replaced the first 103 amino acids of Tmem2, corresponding to its cytoplasmic and transmembrane domains, with the first 23 amino acids of zebrafish Sonic Hedgehog (Ekker et al., 1995), which serve as a signal to target the ectodomain for secretion.

Imaging

Fluorescent images are maximal intensity projections of confocal reconstructions, with the exception of the single optical slices shown in Fig. 3A-E. *Z*-stacks containing 120-140 slices (0.5 µm thick) were acquired with a 25× water objective on a Leica SP5 microscope and analyzed with Imaris software (Bitplane). Additional images were captured using Zeiss Axiozoom and Axioimager microscopes with a Zeiss AxioCam and processed using Zeiss AxioVision and Adobe Creative Suite.

Acknowledgements

We thank L. Pandolfo and K. Garske for expert zebrafish care, C. Henry for helpful input, and members of the Yelon lab for constructive discussions.

Competing interests

The authors declare no competing or financial interests.

Author contributions

L.R., L.H. and D.Y. designed these studies; L.R., L.H., C.W. and J.P. performed experiments and analyzed data; and L.R. and D.Y. wrote the manuscript with input from all authors.

Funding

This work was supported by grants to D.Y. from the National Institutes of Health (NIH) [R01 HL069594; R01 HL133166] and the March of Dimes Foundation [1-FY08-589], by fellowship support to L.R. from the Association Française contre les Myopathies [MNM1 2013–16528] and the American Heart Association with The Children's Heart Foundation [13POST16870010, 15POST25080308] and by

fellowship support to L.H. from the UCSD Cell and Molecular Genetics Training Program [NIH T32 GM007240] and the American Heart Association [15PRE22480001]. Deposited in PMC for release after 12 months.

Supplementary information

Supplementary information available online at
http://dev.biologists.org/lookup/doi/10.1242/dev.139485.supplemental

References

Arrington, C. B. and Yost, H. J. (2009). Extra-embryonic syndecan 2 regulates organ primordia migration and fibrillogenesis throughout the zebrafish embryo. *Development* **136**, 3143-3152.

Barresi, M. J., Stickney, H. L. and Devoto, S. H. (2000). The zebrafish slow-muscle-omitted gene product is required for Hedgehog signal transduction and the development of slow muscle identity. *Development* **127**, 2189-2199.

Bassett, D. I., Bryson-Richardson, R. J., Daggett, D. F., Gautier, P., Keenan, D. G. and Currie, P. D. (2003). Dystrophin is required for the formation of stable muscle attachments in the zebrafish embryo. *Development* **130**, 5851-5860.

Berger, J. and Currie, P. D. (2012). Zebrafish models flex their muscles to shed light on muscular dystrophies. *Dis. Model. Mech.* **5**, 726-732.

Bertini, E., D'Amico, A., Gualandi, F. and Petrini, S. (2011). Congenital muscular dystrophies: a brief review. *Semin. Pediatr. Neurol.* **18**, 277-288.

Blagden, C. S., Currie, P. D., Ingham, P. W. and Hughes, S. M. (1997). Notochord induction of zebrafish slow muscle mediated by Sonic hedgehog. *Genes Dev.* **11**, 2163-2175.

Bouchet-Séraphin, C., Vuillaumier-Barrot, S. and Seta, N. (2015). Dystroglycanopathies: about numerous genes involved in glycosylation of one single glycoprotein. *J. Neuromuscul. Dis.* **2**, 27-38.

Bryson-Richardson, R. J. and Currie, P. D. (2008). The genetics of vertebrate myogenesis. *Nat. Rev. Genet.* **9**, 632-646.

Buckingham, M. and Vincent, S. D. (2009). Distinct and dynamic myogenic populations in the vertebrate embryo. *Curr. Opin. Genet. Dev.* **19**, 444-453.

Charvet, B., Ruggiero, F. and Le Guellec, D. (2012). The development of the myotendinous junction. A review. *Muscles Ligaments Tendons J.* **2**, 53-63.

Crawford, B. D., Henry, C. A., Clason, T. A., Becker, A. L. and Hille, M. B. (2003). Activity and distribution of paxillin, focal adhesion kinase, and cadherin indicate cooperative roles during zebrafish morphogenesis. *Mol. Biol. Cell* **14**, 3065-3081.

Ekker, S. C., Ungar, A. R., Greenstein, P., von Kessler, D. P., Porter, J. A., Moon, R. T. and Beachy, P. A. (1995). Patterning activities of vertebrate hedgehog proteins in the developing eye and brain. *Curr. Biol.* **5**, 944-955.

Ervasti, J. M. and Campbell, K. P. (1993). Dystrophin and the membrane skeleton. *Curr. Opin. Cell Biol.* **5**, 82-87.

Garavito-Aguilar, Z. V., Riley, H. E. and Yelon, D. (2010). Hand2 ensures an appropriate environment for cardiac fusion by limiting Fibronectin function. *Development* **137**, 3215-3220.

Gibbs, E. M., Horstick, E. J. and Dowling, J. J. (2013). Swimming into prominence: the zebrafish as a valuable tool for studying human myopathies and muscular dystrophies. *FEBS J.* **280**, 4187-4197.

Godfrey, C., Foley, A. R., Clement, E. and Muntoni, F. (2011). Dystroglycanopathies: coming into focus. *Curr. Opin. Genet. Dev.* **21**, 278-285.

Goody, M. F., Kelly, M. W., Lessard, K. N., Khalil, A. and Henry, C. A. (2010). Nrk2b-mediated NAD+ production regulates cell adhesion and is required for muscle morphogenesis in vivo: Nrk2b and NAD+ in muscle morphogenesis. *Dev. Biol.* **344**, 809-826.

Goody, M. F., Kelly, M. W., Reynolds, C. J., Khalil, A., Crawford, B. D. and Henry, C. A. (2012). NAD+ biosynthesis ameliorates a zebrafish model of muscular dystrophy. *PLoS Biol.* **10**, e1001409.

Goody, M. F., Sher, R. B. and Henry, C. A. (2015). Hanging on for the ride: adhesion to the extracellular matrix mediates cellular responses in skeletal muscle morphogenesis and disease. *Dev. Biol.* **401**, 75-91.

Hall, T. E., Bryson-Richardson, R. J., Berger, S., Jacoby, A. S., Cole, N. J., Hollway, G. E., Berger, J. and Currie, P. D. (2007). The zebrafish candyfloss mutant implicates extracellular matrix adhesion failure in laminin alpha2-deficient congenital muscular dystrophy. *Proc. Natl. Acad. Sci. USA* **104**, 7092-7097.

Hori, Y. S., Kuno, A., Hosoda, R., Tanno, M., Miura, T., Shimamoto, K. and Horio, Y. (2011). Resveratrol ameliorates muscular pathology in the dystrophic mdx mouse, a model for Duchenne muscular dystrophy. *J. Pharmacol. Exp. Ther.* **338**, 784-794.

Jackson, H. E. and Ingham, P. W. (2013). Control of muscle fibre-type diversity during embryonic development: the zebrafish paradigm. *Mech. Dev.* **130**, 447-457.

Jacoby, A. S., Busch-Nentwich, E., Bryson-Richardson, R. J., Hall, T. E., Berger, J., Berger, S., Sonntag, C., Sachs, C., Geisler, R., Stemple, D. L. et al. (2009). The zebrafish dystrophic mutant softy maintains muscle fibre viability despite basement membrane rupture and muscle detachment. *Development* **136**, 3367-3376.

Jenkins, M. H., Alrowaished, S. S., Goody, M. F., Crawford, B. D. and Henry, C. A. (2016). Laminin and Matrix metalloproteinase 11 regulate Fibronectin levels in the zebrafish myotendinous junction. *Skeletal Muscle* **6**, 18.

Kanagawa, M., Michele, D. E., Satz, J. S., Barresi, R., Kusano, H., Sasaki, T., Timpl, R., Henry, M. D. and Campbell, K. P. (2005). Disruption of perlecan binding and matrix assembly by post-translational or genetic disruption of dystroglycan function. *FEBS Lett.* **579**, 4792-4796.

Kawahara, G., Guyon, J. R., Nakamura, Y. and Kunkel, L. M. (2010). Zebrafish models for human FKRP muscular dystrophies. *Hum. Mol. Genet.* **19**, 623-633.

Kirschner, J. (2013). Congenital muscular dystrophies. *Handb. Clin. Neurol.* **113**, 1377-1385.

Lin, Y.-Y., White, R. J., Torelli, S., Cirak, S., Muntoni, F. and Stemple, D. L. (2011). Zebrafish Fukutin family proteins link the unfolded protein response with dystroglycanopathies. *Hum. Mol. Genet.* **20**, 1763-1775.

Michele, D. E., Barresi, R., Kanagawa, M., Saito, F., Cohn, R. D., Satz, J. S., Dollar, J., Nishino, I., Kelley, R. I., Somer, H. et al. (2002). Post-translational disruption of dystroglycan-ligand interactions in congenital muscular dystrophies. *Nature* **418**, 417-422.

Moore, C. J. and Winder, S. J. (2012). The inside and out of dystroglycan post-translational modification. *Neuromuscul. Disord.* **22**, 959-965.

Muntoni, F., Torelli, S. and Brockington, M. (2008). Muscular dystrophies due to glycosylation defects. *Neurotherapeutics* **5**, 627-632.

Rampoldi, E., Meola, G., Conti, A. M., Velicogna, M. and Larizza, L. (1986). A comparative analysis of collagen III, IV, laminin and fibronectin in Duchenne muscular dystrophy biopsies and cell cultures. *Eur. J. Cell Biol.* **42**, 27-34.

Sciandra, F., Bozzi, M., Bigotti, M. G. and Brancaccio, A. (2013). The multiple affinities of alpha-dystroglycan. *Curr. Protein Pept. Sci.* **14**, 626-634.

Smith, K. A., Lagendijk, A. K., Courtney, A. D., Chen, H., Paterson, S., Hogan, B. M., Wicking, C. and Bakkers, J. (2011). Transmembrane protein 2 (Tmem2) is required to regionally restrict atrioventricular canal boundary and endocardial cushion development. *Development* **138**, 4193-4198.

Snow, C. J. and Henry, C. A. (2009). Dynamic formation of microenvironments at the myotendinous junction correlates with muscle fiber morphogenesis in zebrafish. *Gene Expr. Patterns* **9**, 37-42.

Snow, C. J., Goody, M., Kelly, M. W., Oster, E. C., Jones, R., Khalil, A. and Henry, C. A. (2008a). Time-lapse analysis and mathematical characterization elucidate novel mechanisms underlying muscle morphogenesis. *PLoS Genet.* **4**, e1000219.

Snow, C. J., Peterson, M. T., Khalil, A. and Henry, C. A. (2008b). Muscle development is disrupted in zebrafish embryos deficient for fibronectin. *Dev. Dyn.* **237**, 2542-2553.

Thorsteinsdóttir, S., Deries, M., Cachaço, A. S. and Bajanca, F. (2011). The extracellular matrix dimension of skeletal muscle development. *Dev. Biol.* **354**, 191-207.

Totong, R., Schell, T., Lescroart, F., Ryckebusch, L., Lin, Y.-F., Zygmunt, T., Herwig, L., Krudewig, A., Gershoony, D., Belting, H.-G. et al. (2011). The novel transmembrane protein Tmem2 is essential for coordination of myocardial and endocardial morphogenesis. *Development* **138**, 4199-4205.

Trinh, L. A. and Stainier, D. Y. R. (2004). Fibronectin regulates epithelial organization during myocardial migration in zebrafish. *Dev. Cell* **6**, 371-382.

Wells, L. (2013). The o-mannosylation pathway: glycosyltransferases and proteins implicated in congenital muscular dystrophy. *J. Biol. Chem.* **288**, 6930-6935.

Yelon, D., Horne, S. A. and Stainier, D. Y. R. (1999). Restricted expression of cardiac myosin genes reveals regulated aspects of heart tube assembly in zebrafish. *Dev. Biol.* **214**, 23-37.

Zacharias, U., Purfürst, B., Schöwel, V., Morano, I., Spuler, S. and Haase, H. (2011). Ahnak1 abnormally localizes in muscular dystrophies and contributes to muscle vesicle release. *J. Muscle Res. Cell Motil.* **32**, 271-280.

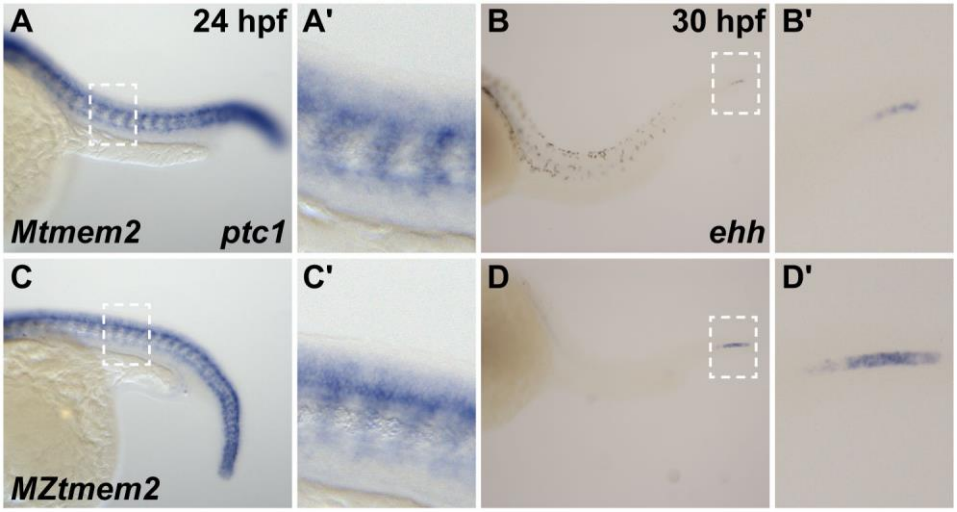

Fig. S1. Hedgehog signaling and notochord differentiation are intact in *MZtmem2* mutants. (**A-D**) In situ hybridization depicts expression of *ptc1* at 24 hpf (A,C) or *ehh* at 30 hpf (B,D) in *Mtmem2* (A,B) and *MZtmem2* (C,D) siblings, lateral views, anterior at left. A'-D' show closer views of regions outlined by white rectangles in A-D. (A,C) Expression of *ptc1* serves as a reporter of Hedgehog signaling. Loss of Hedgehog signaling causes formation of U-shaped somites (Lewis et al., 1999; Schauerte et al., 1998; van Eeden et al., 1996), but Hedgehog signal transduction seems relatively robust in *MZtmem2* mutants. (B,D) Notochord maturation is accompanied by loss of expression of *ehh*, a chordamesoderm marker (Parsons et al., 2002; Stemple, 2005). As notochord differentiation proceeds from anterior to posterior, *ehh* is visible only at the caudal end of the notochord by 30 hpf (B). The progression of differentiation is relatively normal in *MZtmem2* mutants (D), although the slightly increased extent of *ehh* expression that remains at 30 hpf suggests a slight delay.

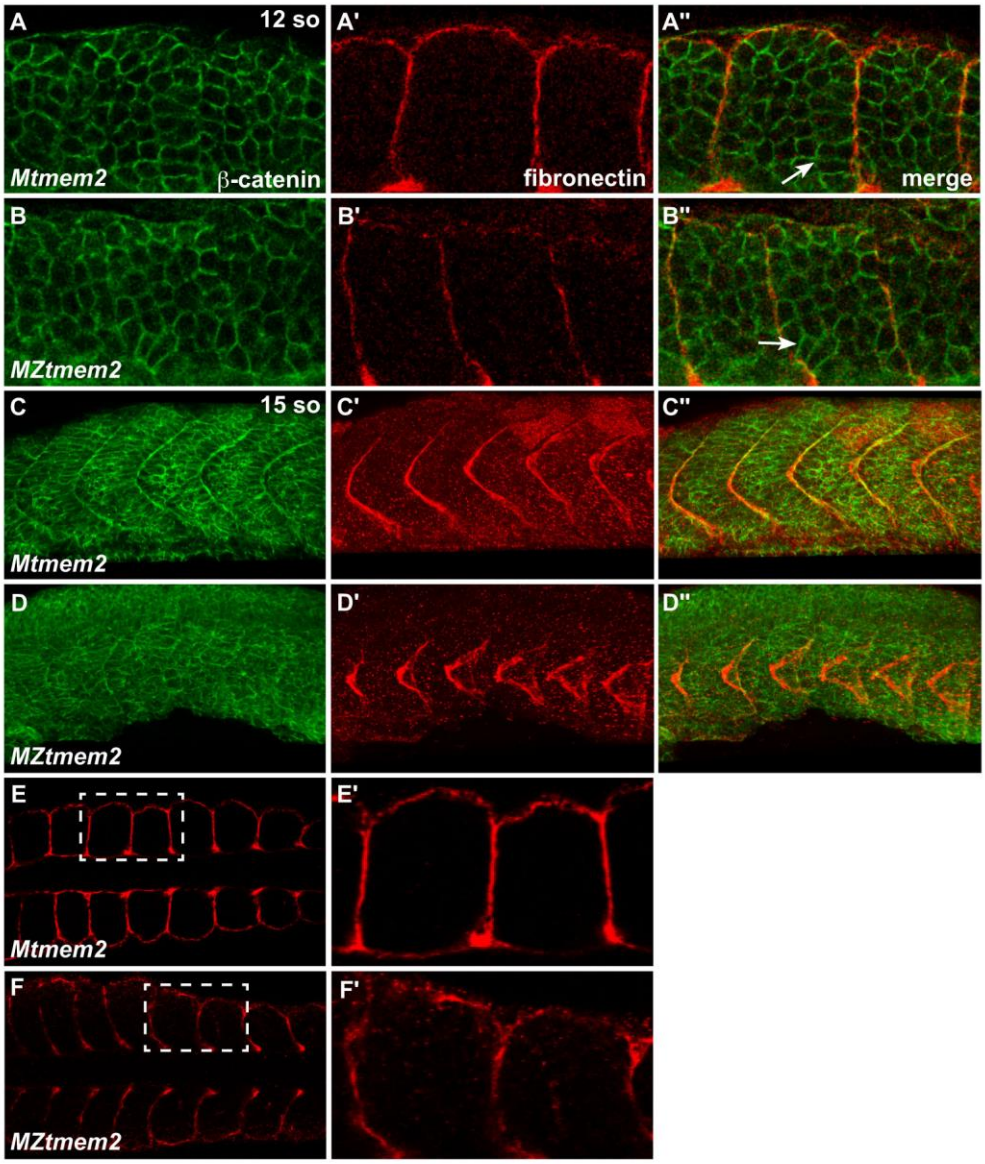

Fig. S2. Initial formation of somite borders appears normal in *MZtmem2* mutants. (**A-F**) Immunofluorescence indicates localization of fibronectin (red) relative to β-catenin (green) at 12 so (A-B) and 15 so (C-F). (A-B) Dorsal views, anterior to the left, of the right myotome show fibronectin localization at somite boundaries. In *MZtmem2* mutants (B'), fibronectin is deposited at each somite boundary, in a pattern comparable to that seen in *Mtmem2* siblings (A'). Additionally, muscle precursor cells at the borders of *MZtmem2* somites exhibit characteristic elongation indicative of the formation of epithelial somite boundaries (Henry et al., 2005) (B'', arrow), just as in *Mtmem2* siblings (A'', arrow). These results suggest that the initial formation of somite boundaries proceeds normally in *MZtmem2* mutants. (C-D) Lateral views, dorsal up, display

fibronectin localization at somite boundaries at 15 so, when the earliest aberrations in fibronectin organization appear in *MZtmem2* mutants. In *MZtmem2* mutants (D'), fibronectin is present at somite boundaries, but seems disorganized, in contrast to the sharply defined fibronectin deposition present in *Mtmem2* siblings (C'). (E-F) Dorsal views, anterior to the left, indicate that fibronectin is present at somite boundaries at 15 so in *MZtmem2* mutants (F), as it is in *Mtmem2* siblings (E). E' and F' show closer views of regions outlined by white rectangles in E and F.

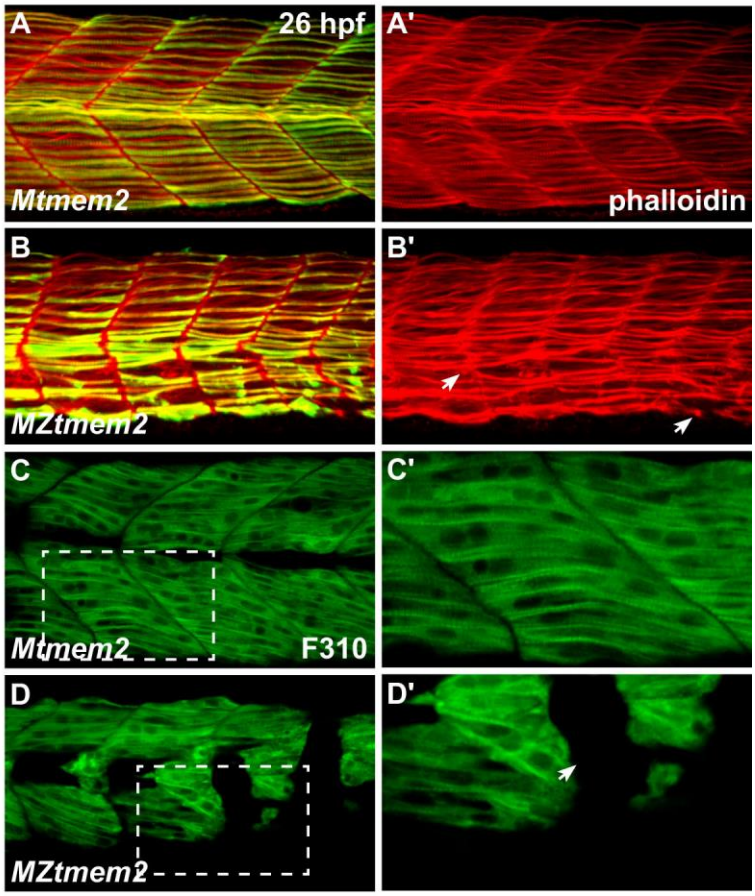

Fig. S3. Disruption of fast muscle fiber attachment in *MZtmem2* mutants. (**A-D**) Immunofluorescence reveals muscle fiber organization, using phalloidin (red in A,B) to recognize both fast and slow fibers, F59 (green in A,B) to recognize slow fibers (Devoto et al., 1996), and F310 (green in C,D) to recognize fast fibers (Nord et al., 2014); lateral views, dorsal up, at 26 hpf. (A,B) In addition to exhibiting detachment of $F59^{+}$ slow muscle fibers (B); see also Fig. 1H), *MZtmem2* mutants display detachment of $F59^{-}$ fast muscle fibers (arrows, B'), in contrast to the attached fibers observed in *Mtmem2* siblings (A). (C,D) Similarly, *MZtmem2* mutants (D) display detachment of $F310^{+}$ fast muscle fibers (arrow, D2), in contrast to the attachment seen in *Mtmem2* siblings (C). C' and D' show closer views of regions outlined by white rectangles in C and D.

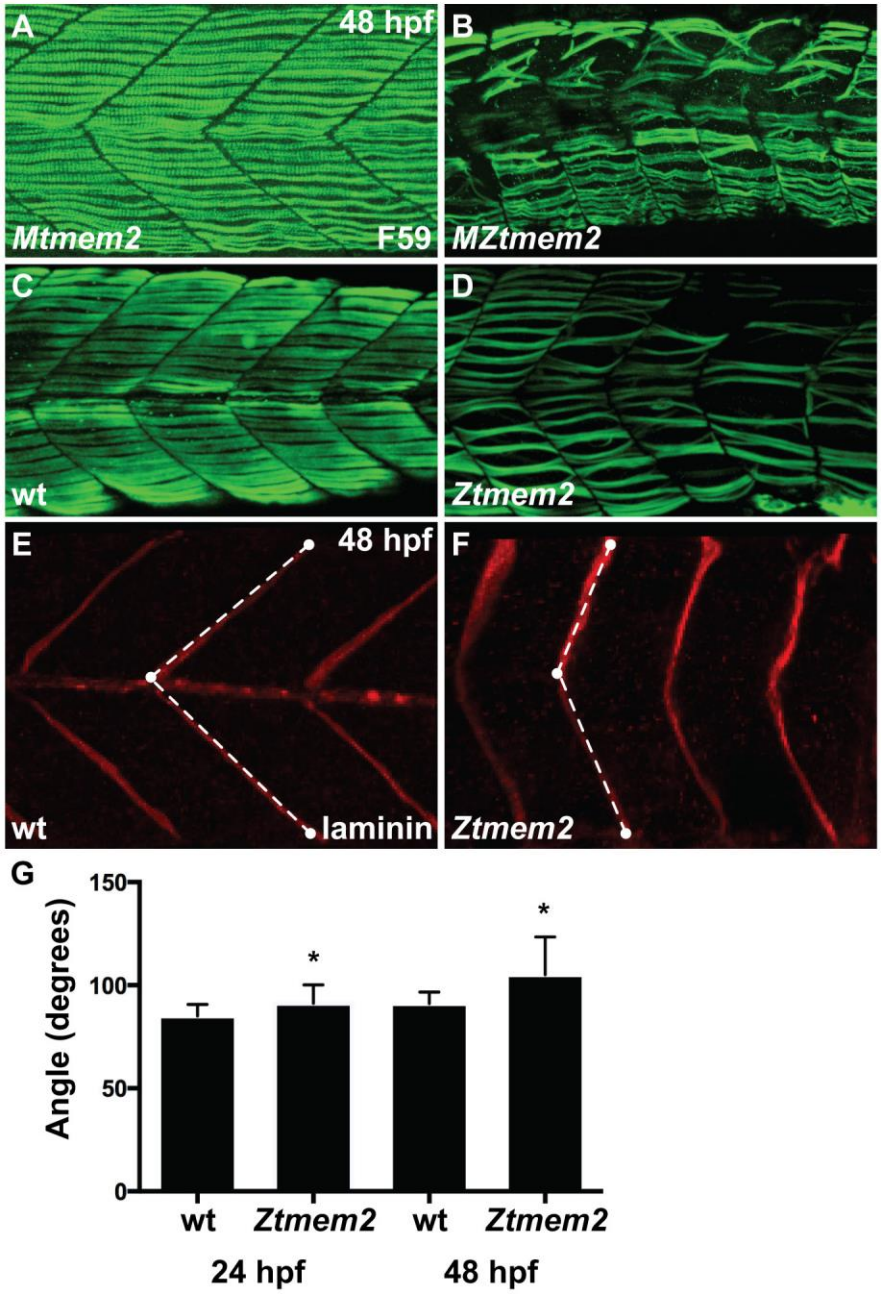

Fig. S4. Impairment of muscle fiber organization in zygotic *tmem2* mutants. (**A-D**) Immunofluorescence with F59 (green) reveals slow muscle fiber organization; lateral views with dorsal up at 48 hpf. At this stage, *MZtmem2* mutants (B) exhibit detachment and disorganization of slow muscle fibers, in contrast to the normal attachment seen in their *Mtmem2* siblings (A). Although we have not observed muscle fiber detachment in zygotic *tmem2* (*Ztmem2*) mutants at 24 hpf (data not shown), we have found fiber detachment and disorganization in some *Ztmem2* mutants (D) by 48 hpf (n=4 out of 33

Ztmem2 mutants examined). (**E,F**) Immunofluorescence detecting laminin (red) deposition at the MTJ reveals somite shape defects in *Ztmem2* mutants. In wild-type (E) and *Ztmem2* (F) sibling embryos, somite shape was evaluated by measuring the angle formed at the MTJ. White dots represent examples of the reference points chosen at the horizontal myoseptum, the dorsal edge of the MTJ, and the ventral edge of the MTJ; dashed lines represent the angle measured using ImageJ software. (**G**) Bar graph compares average angles formed at the MTJ in wild-type and *Ztmem2* embryos at 24 hpf and 48 hpf (in wild-type, n=85 at 24 hpf and n=75 at 48 hpf; in *Ztmem2*, n=52 at 24 hpf and n=154 at 48 hpf). Error bars indicate s.d., and asterisks indicate a significant difference from wild-type (Student's t-test; $p<0.0001$). Somite shapes in *Ztmem2* mutants become less chevron-shaped and more U-shaped over time, presumably as maternal supplies of *tmem2* are depleted and muscle fiber defects accumulate.

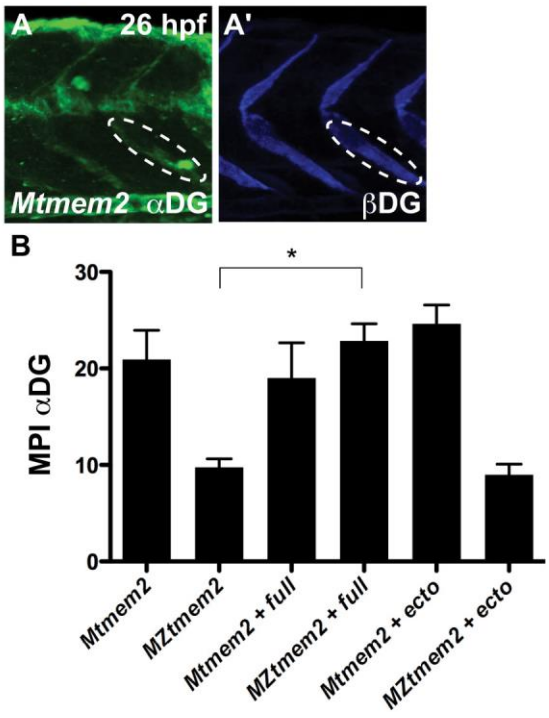

Fig. S5. Quantification of intensity of immunostaining for dystroglycan at the MTJ. (**A)** Confocal reconstruction depicts immunostaining for glycosylated αDG (A) and βDG (A') in a *Mtmem2* embryo at 26 hpf; lateral view, dorsal up. To quantify the intensity of immunostaining through the entire depth of the confocal stack, we used Imaris software to rotate each reconstruction 30 degrees toward the right and then used ImageJ software to measure the mean pixel intensity (MPI) within an oval-shaped region of interest positioned at the MTJ. Ovals of the same size and in the same position were used to measure MPI for both glycosylated αDG and βDG (as outlined in A and A'). (**B**) Bar graph compares MPI of immunostaining for glycosylated αDG at the MTJ at 26 hpf; error bars indicate s.e.m. For each condition, we measured the MPI at 5 different MTJs in each of 3 representative embryos (*Mtmem2*: 2 embryos presenting normal staining and 1 embryo presenting traces of staining; *MZtmem2*: 2 embryos presenting traces of staining and 1 embryo presenting no staining; *Mtmem2* + full: 2 embryos presenting normal staining and 1 embryo presenting traces of staining; *MZtmem2* + full: 3 embryos presenting normal staining; *Mtmem2* + ecto: 3 embryos presenting normal staining; *MZtmem2* + ecto: 2 embryos presenting traces of staining and 1 embryo presenting no staining). Introduction of full-length Tmem2, but not the Tmem2 ectodomain, caused evident improvement in αDG glycosylation in *MZtmem2* mutants. Asterisk indicates significant difference from *MZtmem2* (Student's t-test; $p<0.01$). See also Fig. 4H and Table S3.

SUPPLEMENTAL REFERENCES

Devoto, S. H., Melancon, E., Eisen, J. S. and Westerfield, M. (1996). Identification of separate slow and fast muscle precursor cells in vivo, prior to somite formation. *Development* **122**, 3371-3380.

Henry, C. A., McNulty, I. M., Durst, W. A., Munchel, S. E. and Amacher, S. L. (2005). Interactions between muscle fibers and segment boundaries in zebrafish. *Dev. Biol.* **287**, 346-360.

Lewis, K. E., Currie, P. D., Roy, S., Schauerte, H., Haffter, P. and Ingham, P. W. (1999). Control of muscle cell-type specification in the zebrafish embryo by Hedgehog signalling. *Dev. Biol.* **216**, 469-480.

Nord, H., Burguiere, A. C., Muck, J., Nord, C., Ahlgren, U. and von Hofsten, J. (2014). Differential regulation of myosin heavy chains defines new muscle domains in zebrafish. *Mol. Biol. Cell* **25**, 1384-1395.

Parsons, M. J., Pollard, S. M., Saude, L., Feldman, B., Coutinho, P., Hirst, E. M. and Stemple, D. L. (2002). Zebrafish mutants identify an essential role for laminins in notochord formation. *Development* **129**, 3137-3146.

Schauerte, H. E., van Eeden, F. J., Fricke, C., Odenthal, J., Strahle, U. and Haffter, P. (1998). Sonic hedgehog is not required for the induction of medial floor plate cells in the zebrafish. *Development* **125**, 2983-2993.

Stemple, D. L. (2005). Structure and function of the notochord: an essential organ for chordate development. *Development* **132**, 2503-2512.

van Eeden, F. J., Granato, M., Schach, U., Brand, M., Furutani-Seiki, M., Haffter, P., Hammerschmidt, M., Heisenberg, C. P., Jiang, Y. J., Kane, D. A., et al. (1996). Mutations affecting somite formation and patterning in the zebrafish, Danio rerio. *Development* **123**, 153-164.

Table S1. Rescue of muscle fiber attachment by injection of *tmem2* mRNA.

		Muscle fiber phenotype at 48 hpf		
		many detached	few detached	all attached
Mtmem2	uninjected			8/8 (100%)
MZtmem2	uninjected	9/9 (100%)		
Mtmem2	full-length			7/7 (100%)
MZtmem2	full-length	1/17 (6%)	1/17 (6%)	15/17 (88%)
Mtmem2	ectodomain		1/2 (50%)	1/2 (50%)
MZtmem2	ectodomain	2/8 (25%)	3/8 (25%)	3/8 (37.5%)

Summary of 3 independent experiments evaluating whether injection of mRNA encoding either full-length Tmem2 or the Tmem2 ectodomain can rescue the muscle fiber detachment defects in *MZtmem2* mutants. Genotype (*Mtmem2* and *MZtmem2*) and mRNA injected (uninjected, full-length, or ectodomain) are provided for each set of embryos. Data indicate the fraction of examined embryos displaying severe muscle fiber detachment, a small number of detached fibers, or normal fiber attachment. For each embryo, we examined 11 somites on the left side of the myotome, using immunofluorescence with F59 and phalloidin to reveal muscle fiber organization. Embryos were classified as "many detached" if fiber detachment was evident in all 11 somites examined and as "few detached" if fiber detachment was evident in 5 or fewer somites. In a subset of these embryos, we counted the numbers of attached and detached $F59^{+}$ fibers within the 11 somites examined, and this quantification is presented in Fig. 1L. Full-length Tmem2 and the Tmem2 ectodomain are both capable of rescuing muscle fiber attachment in *MZtmem2* mutants, although full-length Tmem2 seems to rescue more efficiently.

Table S2. Rescue of cardiac fusion by injection of *tmem2* mRNA.

		Cardiac fusion phenotype at 24 hpf			
		cardia bifida	partial fusion	cardiac ring	heart tube
Mtmem2	uninjected				8/8 (100%)
MZtmem2	uninjected	19/23 (83%)	4/23 (17%)		
Mtmem2	full-length				27/27 (100%)
MZtmem2	full-length			4/18 (22%)	14/18 (78%)
Mtmem2	ectodomain		1/13 (8%)		12/13 (92%)
MZtmem2	ectodomain	2/28 (7%)	7/28 (25%)	17/28 (61%)	2/28 (7%)

Summary of 4 independent experiments evaluating whether injection of mRNA encoding either full-length Tmem2 or the Tmem2 ectodomain can rescue the cardiac fusion defects in *MZtmem2* mutants. Genotype (*Mtmem2* and *MZtmem2*) and mRNA injected (uninjected, full-length, or ectodomain) are provided for each set of embryos. Cardiac phenotypes were assessed through in situ hybridization for *myl7*, as in Fig. 3F-K. Data indicate the fraction of examined embryos displaying cardia bifida (as in Fig. 3G), partial fusion at the posterior end of the cardiac primordia (as in Fig. 3H), fusion to form a ring of cardiomyocytes (as in Fig. 3K), or normal heart tube assembly (as in Fig. 3J). Full-length Tmem2 and the Tmem2 ectodomain are both capable of rescuing cardiac fusion in *MZtmem2* mutants, although full-length Tmem2 seems to rescue more efficiently.

Table S3. Rescue of αDG glycosylation by injection of *tmem2* mRNA.

		IIH6 staining at 26 hpf		
		no staining	traces of staining	normal staining
Mtmem2	uninjected		4/26 (15%)	22/26 (85%)
MZtmem2	uninjected	18/32 (56%)	14/32 (44%)	
Mtmem2	full-length		1/9 (11%)	8/9 (89%)
MZtmem2	full-length		2/13 (15%)	11/13 (85%)
Mtmem2	ectodomain			5/5 (100%)
MZtmem2	ectodomain	1/7 (14%)	6/7 (86%)	

Summary of 3 independent experiments evaluating whether injection of mRNA encoding either full-length Tmem2 or the Tmem2 ectodomain can rescue αDG glycosylation at the MTJ in *MZtmem2* mutants. Genotype (*Mtmem2* and *MZtmem2*) and mRNA injected (uninjected, full-length, or ectodomain) are provided for each set of embryos. αDG glycosylation was assessed through immunostaining with the antibody IIH6, as in Fig. 4E'-G'. Data indicate the fraction of examined embryos displaying no IIH6 staining at the MTJ, trace amounts of IIH6 staining at the MTJ (as in Fig. 4F'), or normal IIH6 staining at the MTJ (as in Fig. 4E' and 4G'). In a subset of these embryos, we measured the intensity of IIH6 staining at 5 different MTJs in each of 3 representative embryos; the results of this quantitative analysis are presented in Figs. 4H and S5. Full-length Tmem2 is capable of rescuing αDG glycosylation at the MTJ in *MZtmem2* mutants, whereas introduction of the Tmem2 ectodomain is not sufficient to rescue normal levels of glycosylated αDG in this context.

Table S4. Antibodies used for immunofluorescence.

	Antigen	Reagent	Vendor	Dilution
Primary antibodies	Myosin heavy chain	Mouse monoclonal (F59)	Developmental Studies Hybridoma Bank (supernatant)	1:10
	Laminin	Rabbit polyclonal	Sigma (#L9393)	1:100
	Fibronectin	Rabbit polyclonal	Sigma (#F3648)	1:100
	β-catenin	Mouse monoclonal (15B8)	Sigma (#C7207)	1:500
	Tropomyosin	Mouse monoclonal (CH1)	Developmental Studies Hybridoma Bank (supernatant)	1:10
	Paxillin	Mouse monoclonal (349)	BD Biosciences (#612405)	1:50
	FAK [pY^{397}]	Rabbit polyclonal	Invitrogen (#44-624G)	1:50
	Myosin heavy chain	Mouse monoclonal (F310)	Developmental Studies Hybridoma Bank (supernatant)	1:10
	α-dystroglycan	Mouse monoclonal (IIH6-C4)	Santa Cruz Biotechnology (#sc-73586)	1:50
	β-dystroglycan	Mouse monoclonal (43DAG1/8D5)	Novocastra (#NCL-b-DG)	1:50
Secondary antibodies	Rabbit IgG	Goat polyclonal; Alexa Fluor 594	Molecular Probes (#A11012)	1:200
	Rabbit IgG	Goat polyclonal; Alexa Fluor 647	Molecular Probes (#A21245)	1:200
	Mouse IgG1	Goat polyclonal; FITC	Southern Biotechnology (#1070-02)	1:100